

Structural and Magnetic Study of Zn-Substituted NiGa_yFe_{2-y}O₄ Ferrite

A. Hashhash · M. Yehia · S. M. Ismail · S. S. Ata-Allah

Received: 7 May 2014 / Accepted: 18 May 2014 / Published online: 8 June 2014
© Springer Science+Business Media New York 2014

Abstract Single-phase spinel ferrite Ni_{1-x}Zn_xGa_yFe_{2-y}O₄ with (0.0 ≤ *x* ≤ 0.5) and *y* = 0.5 samples were synthesized using solid-state reaction technique. These ferrites were investigated using X-ray diffraction (XRD), vibrating sample magnetometer (VSM) and Mössbauer effect (ME) spectroscopy. XRD patterns confirmed the formation of single-phase cubic spinel ferrites for all samples. Lattice parameter was found to decrease with the introduction of Ga³⁺ in NiFe₂O₄, and then to increase with the increasing of Zn²⁺ content *x*. ME measurements illustrated a strong dependence on the zinc concentration. The cation distribution calculated from the ME spectra at room temperature indicated that the Ga³⁺ ion substituted iron in both octahedral B and tetrahedral A- sites. Zn²⁺ ions firstly introduced in A- site, and for higher *x*, they distribute in both B- and A- sites. VSM measurements indicated that the change in the value of saturation magnetization can be explained using the cation distribution obtained from ME measurements. The coercivity values can be interpreted on the basis of magneto-crystalline anisotropy.

Keywords Ni ferrite · XRD · VSM · Mössbauer effect spectroscopy

1 Introduction

Ferrimagnetic spinel ferrites are important magnetic materials, which are widely used in high-frequency devices due to their high permeability in the radio frequency region,

high electrical resistance, mechanical hardness, and chemical stability [1]. Spinel ferrite chemical formula is MFe₂O₄, where M represents a divalent transition metal ion. In this structure, oxygen ions form face centered cubic lattice and the metal ions are surrounded by either 4 (tetrahedral) or 6 (octahedral) oxygen ions. The properties of these materials depend upon the distribution of cation (metal ions) between tetrahedral (A)- and octahedral [B]- sites. Cation distribution in these systems is very much sensitive to the method of preparation, particle size, and doping. Hence, the electrical, magnetic and optical properties of ferrites can be tuned by the type and amount of substituting elements [2–4]. Substitutions of nonmagnetic ions in spinel ferrites have received a great interest because they alter the magnetic and electric properties. This isomorphous substitutions are particularly apparent in the Mössbauer effect spectra, where the magnetic interactions drastically reduced, resulting in the lower magnetic ordering and decreased the hyperfine fields [5, 6]. The present work reports the preparation procedures and the results of X-ray diffraction (XRD), vibrating sample magnetometer (VSM), and Mössbauer effect (ME) spectroscopy measurements of the spinel ferrites Ni_{1-x}Zn_xGa_yFe_{2-y}O₄ with (0.0 ≤ *x* ≤ 0.5) and *y* = 0.5, aiming to shed more lights on the microscopic picture of the structure parameters and magnetic properties in this diluted ferrimagnets.

2 Experimental Details

Polycrystalline samples of the studied compounds were prepared using the solid-state reaction method. The powders of NiO, ZnO, Ga₂O₃, and Fe₂O₃ oxides (with purity 99.99 %) in the required stoichiometric proportions were thoroughly mixed and milled. The mixture is pre-sintered at (1,000–1,150 °C), depending on the ZnO content, for 60 h, then

A. Hashhash · M. Yehia (✉) · S. M. Ismail · S. S. Ata-Allah
Reactor Physics Department, Nuclear Research Center, Atomic Energy Authority, P.O. Box 13759, Cairo, Egypt
e-mail: m6yehia@yahoo.com

slowly cooled to room temperature. The product is reground and fired again under the same conditions to improve homogeneity. X-ray diffraction patterns of the prepared samples were recorded at room temperature using monochromatic $\text{CuK}\alpha$ radiation (with $\lambda = 1.5418 \text{ \AA}$). The crystallographic parameters: lattice constant (a), ionic radius per molecule of the tetrahedral and octahedral sites (r_A, r_B), bond length in the two crystallographic sites (R_A and R_B) and oxygen position parameter (u) have been calculated. Austin Science Mössbauer Spectrometer with constant acceleration and data acquisition system is used in a standard transmission setup with a Personal Computer Analyzer (PCA II card with 1,024 channels). The radioactive source is ^{57}Co imbedded in Rh matrix with initial activity of 50 mCi. Metallic iron spectrum is used for the calibration of both observed velocities and hyperfine magnetic fields. The absorber thickness is approximately 10 mg cm^{-2} of natural iron. The cation distributions and all ME parameters are calculated from the recorded Mössbauer spectra [9]. Magnetic measurements on the prepared ferrites were carried out using vibrating sample magnetometer (VSM; 9600-1 LDJ, USA) with a maximum applied field of nearly 20 kG at room temperature and the saturation magnetization M_s and the coercivity H_c were determined.

3 Results and Discussion

3.1 X-ray Measurements

The X-ray diffraction patterns of $\text{Ni}_{1-x}\text{Zn}_x\text{Ga}_y\text{Fe}_{2-y}\text{O}_4$ with ($y = 0.5$ and $0.0 \leq x \leq 0.5$) samples are shown in Fig. 1. XRD patterns confirm the formation of single-phase face center cubic (FCC) spinel structures with $Fd\bar{3}m$ space group, and no diffraction lines attributed to the presence of impurities or metal oxides were observed. As illustrated in Fig. 2, the partial replacement of Fe^{3+} by Ga^{3+} in NiFe_2O_4 causes a decrease in the lattice constant (a). However, by replacing Ni^{2+} by Zn^{2+} , a gradual increase in the lattice constant is observed. The lattice parameter a can be calculated theoretically based on the cation distribution obtained from Mössbauer effect spectroscopy (Section 3.3). The values of mean ionic radius per molecule of the A-site (r_A) and B-site (r_B) are given by the following relationships [8]:

$$r_A = C_{\text{Fe}}r(\text{Fe}^{3+}) + C_{\text{Ni}}r(\text{Ni}^{2+}) + C_{\text{Ga}}r(\text{Ga}^{3+}) + C_{\text{Zn}}r(\text{Zn}^{2+}) \quad (1)$$

$$r_B = \frac{1}{2} \left[C_{\text{Fe}}r(\text{Fe}^{3+}) + C_{\text{Ni}}r(\text{Ni}^{2+}) + C_{\text{Ga}}r(\text{Ga}^{3+}) + C_{\text{Zn}}r(\text{Zn}^{2+}) \right] \quad (2)$$

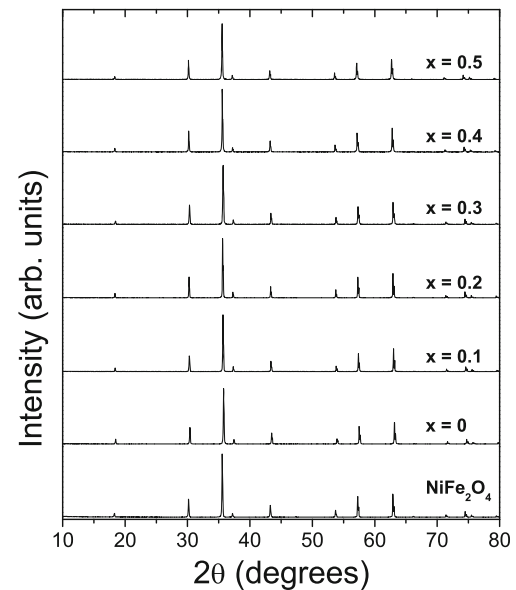


Fig. 1 X-ray diffraction patterns at room temperature for NiFe_2O_4 and $\text{Ni}_{1-x}\text{Zn}_x\text{Ga}_{0.5}\text{Fe}_{1.5}\text{O}_4$ spinel ferrites

where $r(\text{Fe}^{3+})$, $r(\text{Ni}^{2+})$, $r(\text{Ga}^{3+})$, and $r(\text{Zn}^{2+})$ are the ionic radii of Fe^{3+} , Ni^{2+} , Ga^{3+} , and Zn^{2+} ions given in Table 1. While C_{Fe} , C_{Ni} , C_{Ga} , and C_{Zn} are the concentration of the mentioned ions in A- and B- sites, respectively. The concentration of each ion in both A and B- sites are taken from ME results. The average (A-O) and (B-O) bond lengths are R_A and R_B , respectively, and are given by:

$$R_A = r_A + r_o \quad \text{and} \quad R_B = r_B + r_o \quad (3)$$

where $r_o = 1.32 \text{ \AA}$ is the radius of oxygen ion. The lattice parameter a_{th} can be obtained from the following:

$$a_{\text{th}} = \frac{8}{3\sqrt{3}} \left[(r_A + r_o) + \sqrt{3}(r_B + r_o) \right] \quad (4)$$

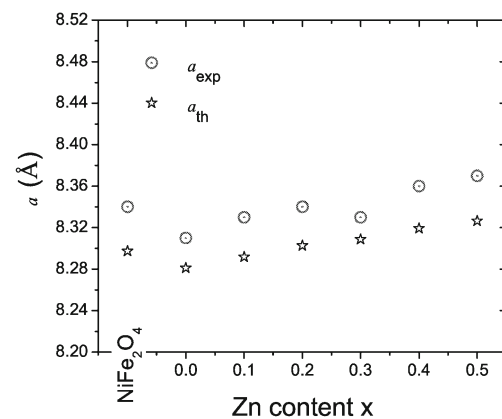


Fig. 2 Variation of the lattice parameters (a) for NiFe_2O_4 and $\text{Ni}_{1-x}\text{Zn}_x\text{Ga}_{0.5}\text{Fe}_{1.5}\text{O}_4$ spinel ferrites. a_{exp} is the lattice parameter obtained from the XRD measurements and a_{th} is the lattice parameter calculated according to the cation distribution obtained from the Mössbauer effect measurements

Table 1 The effective ionic radii of $r(\text{Fe}^{3+})$, $r(\text{Ni}^{2+})$, $r(\text{Ga}^{3+})$, and $r(\text{Zn}^{2+})$ ions in the tetrahedral A- site and octahedral B- site [7]

| Ion | Tetrahedral A- site (Å) | Octahedral B- site (Å) |
|---------------------|----------------------------|---------------------------|
| $r(\text{Fe}^{3+})$ | 0.49 | 0.645 |
| $r(\text{Ni}^{2+})$ | 0.55 | 0.69 |
| $r(\text{Ga}^{3+})$ | 0.47 | 0.62 |
| $r(\text{Zn}^{2+})$ | 0.60 | 0.74 |

Table 2 summarizes the calculated values of a_{th} , r_{A} , r_{B} , R_{A} , R_{B} , and u . The experimentally obtained values of the lattice parameter a_{exp} are compared to a_{th} . As shown in Fig. 2, the theoretically calculated values of (a_{th}) are in good agreement with (a_{exp}) and they both have the same trend. For $x = 0$, the cation distribution suggests that Ga^{3+} substitutes Fe^{3+} in both A- and B- sites, and since $r(\text{Ga}^{3+}) < r(\text{Fe}^{3+})$, r_{A} , r_{B} , and the average bond lengths (R_{A} and R_{B}) decrease and consequently the lattice parameter will decrease. By introducing Zn to the system, and since $r(\text{Zn}^{2+}) > r(\text{Ni}^{2+})$, a gradual increase in the lattice parameter with increasing Zn content (x) would be expected. However, the cation distribution suggests a more complicated picture. For $x < 3$, Zn^{2+} goes to A- site and transfers mainly Ga^{3+} to the B- site. The $r(\text{Zn}^{2+})$ is bigger than both $r(\text{Ga}^{3+})$ and $r(\text{Fe}^{3+})$, which leads to an increase in r_{A} and R_{A} accompanied with a decrease in r_{B} and R_{B} . The resultant effect is a gradual increase in the lattice parameter. For $x = 3$, the ME measurements suggest that Zn^{2+} distributes between A- and B- sites and a considerable portion of Zn^{2+} ions substitute Ni^{2+} in the B- sites. This causes an inverse behavior, where r_{A} and R_{A} decrease, while both r_{B} and R_{B} increase and the resultant effect is a slight decrease in the lattice parameter. For $x > 3$, Zn continues to distribute between A- and B- sites. The ionic radius of Zn^{2+} ions in the octahedral coordinates is bigger than that in the tetrahedral coordinates. As a resultant, the lattice parameter increases again for higher Zn content.

Table 2 Experimental (a_{exp}) and theoretical (a_{th}) lattice constants, ionic radii of A- and B- sites (r_{A} and r_{B}), the average bond lengths (R_{A} and R_{B}), and the oxygen positional parameter (u) of NiFe_2O_4 and $\text{Ni}_{1-x}\text{Zn}_x\text{Ga}_{0.5}\text{Fe}_{1.5}\text{O}_4$ spinel ferrites

| x | a_{exp} (Å) | a_{th} (Å) | r_{A} (Å) | R_{A} (Å) | r_{B} (Å) | R_{B} (Å) | $u^{3\text{m}}$ (Å) | $u^{43\text{m}}$ (Å) |
|---------------------------|----------------------|---------------------|--------------------|--------------------|--------------------|--------------------|---------------------|----------------------|
| NiFe_2O_4 | 8.34 | 8.297 | 0.491 | 1.861 | 0.667 | 2.037 | 0.2710 | 0.39599 |
| 0.0 | 8.31 | 8.281 | 0.484 | 1.854 | 0.665 | 2.035 | 0.2712 | 0.39619 |
| 0.1 | 8.33 | 8.292 | 0.497 | 1.867 | 0.661 | 2.031 | 0.2704 | 0.39537 |
| 0.2 | 8.34 | 8.302 | 0.510 | 1.880 | 0.658 | 2.028 | 0.2696 | 0.39457 |
| 0.3 | 8.33 | 8.309 | 0.509 | 1.879 | 0.661 | 2.031 | 0.2698 | 0.39475 |
| 0.4 | 8.36 | 8.319 | 0.522 | 1.892 | 0.657 | 2.027 | 0.2689 | 0.39393 |
| 0.5 | 8.37 | 8.326 | 0.523 | 1.893 | 0.660 | 2.030 | 0.2690 | 0.39397 |

The oxygen positional parameter or anion parameter (u) for each composition was calculated using the following [8]:

$$u^{3\text{m}} = \frac{\frac{1}{4}R^2 - \frac{2}{3} + \left(\frac{11}{48}R^2 - \frac{1}{18}\right)^{\frac{1}{2}}}{2R^2 - 2} \tag{5}$$

$$u^{43\text{m}} = \frac{\frac{1}{2}R^2 - \frac{11}{12} + \left(\frac{11}{48}R^2 - \frac{1}{18}\right)^{\frac{1}{2}}}{2R^2 - 2} \tag{6}$$

The oxygen positional parameter (u) depends on the chemical composition, preparation conditions, and sintering procedure. Taking the center of symmetry at $(\frac{1}{4}\frac{1}{4}\frac{1}{4})$ (origin at B- site), the ideal value of parameter u is 0.25, while assuming center of symmetry at $(\frac{3}{8}\frac{3}{8}\frac{3}{8})$ (origin at A- site), u ideal is 0.375. For these ideal values the arrangement of O^{2-} ions are equals exactly a cubic closed packing, but in actual spinel lattice, this ideal pattern is slightly deformed. As illustrated in the table, both $u^{3\text{m}}$ and $u^{43\text{m}}$ are higher than the ideal values, which means that O^{2-} ions move away from the tetrahedrally coordinated A- site cation along the $\langle 111 \rangle$ directions due to the contraction of the tetrahedral interstices, correspondingly the octahedral B- sites become smaller.

3.2 Mössbauer Effect Measurements

Figure 3 shows room temperature Mössbauer effect measurements of NiFe_2O_4 and $\text{Ni}_{1-x}\text{Zn}_x\text{Ga}_{0.5}\text{Fe}_{1.5}\text{O}_4$ samples. For NiFe_2O_4 , spectrum consists of two clearly split Zeeman sextets due to the almost equally distributed Fe^{3+} ions between A and B- sites. For $0.0 \leq x \leq 0.3$, Mössbauer effect spectra are broadening gradually and each spectra still consists of two Zeeman sextets. By increasing Zn content to $x = 0.4$, in addition to the two sextets, a central quadruple doublet is observed. However, for $x = 0.5$ sample, sextets disappears and two quadruple doublets completely dominate the Mössbauer effect spectrum.

The broadening of Mössbauer effect spectra is expected to develop gradually because of the introduction of two successive nonmagnetic ions (Ga^{3+} and Zn^{2+}) with closed

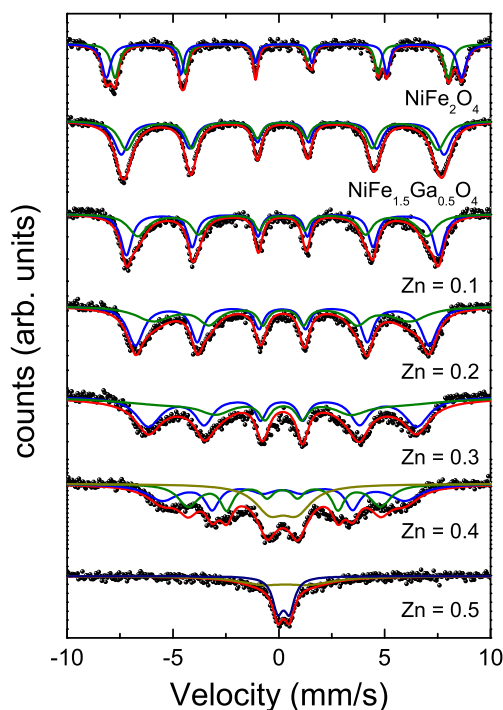


Fig. 3 Mössbauer effect spectra at room temperature of NiFe_2O_4 and $\text{Ni}_{1-x}\text{Zn}_x\text{Ga}_{0.5}\text{Fe}_{1.5}\text{O}_4$

$3d^{10}$ shell. Both Ga^{3+} and Zn^{2+} substitute Fe^{3+} and Ni^{2+} and accordingly will weaken the A-A, B-B, and A-B interactions, which is expected to decrease the transition temperature (T_N). The disappearance of the sextets and the appearance of the quadruple doublets in the $x = 5$ spectrum are a straight forward signature of the paramagnetic nature of this sample.

The hyperfine parameters, isomer shift (δ), quadrupole splitting (ΔE_Q), and hyperfine field (H_f), of all the studied samples are summarized in Table 3. The isomer shifts (δ) of

the sextets lie between 0.13 and 0.25 mm/s, which is typical values of Fe^{3+} ion octahedral and tetrahedral environments. Typically for ferrites, the bond distance $\text{Fe}^{3+}\text{-O}^{2-}$ is larger for the [B] sites than (A) sites. Therefore, the overlapping of Fe ion orbital is small at the B- sites and $\delta_B > \delta_A$ is expected [9, 10]. The developing of isomer shift for different samples tends to have reverse behavior in A and B- sites as illustrated in Fig. 4. By introducing Ga and increasing Zn content x , δ_A increases gradually in the same time δ_B decreases. Such behavior may be connected to the expansion of the A-site suggested by the increase of R_A and the contraction of the B- site illustrated in the decrease of R_B . Generally, the quadrupole splitting (ΔE_Q) has values close to zero for both (A)- and [B]- sites. In the NiFe_2O_4 and $\text{Ni}_{1-x}\text{Zn}_x\text{Ga}_{0.5}\text{Fe}_{1.5}\text{O}_4$ system, ΔE_Q has small values close to zero, but it increases for higher Zn content. Such increase can be explained that by introducing Ga^{3+} and Zn^{2+} ions in both A- and B- sites, it is going to increase chemical disorder in spinel structure, which generates electrical field gradient of varying magnitude, direction, sign, and symmetry [11]. Figure 4 shows that the H_{fB} of the octahedral [B]-site is larger than the H_{fA} of the tetrahedral (A)- site [9, 11]. The hyperfine fields of both A- site and B- sites are decreasing with introducing Ga and Zn. Ga^{3+} and Zn^{2+} ions ($3d^{10}$) have no unpaired d electrons and no magnetic moment, and so Ga^{3+} and Zn^{2+} ions do not participate in the A-A, B-B, and A-B interactions and will destructively affect magnetism and decrease H_f and the transition temperatures.

3.3 Cation Distribution

The cation inversion parameter varies based on a complex set of factors, such as, preparation conditions, the electrostatic contribution to the lattice energy, cationic radii,

Table 3 The isomer shift (δ), quadrupole splitting (ΔE_Q), and hyperfine field (H_f) of NiFe_2O_4 and $\text{Ni}_{1-x}\text{Zn}_x\text{Ga}_{0.5}\text{Fe}_{1.5}\text{O}_4$ samples

| | | Zn content (x) | | | | | | |
|------------------|--------|---------------------------|---------|---------|---------|---------|---------|--------|
| | | NiFe_2O_4 | 0 | 0.1 | 0.2 | 0.3 | 0.4 | 0.5 |
| δ_A | (mm/s) | 0.1362 | 0.156 | 0.156 | 0.1591 | 0.1591 | 0.2152 | |
| δ_B | (mm/s) | 0.2417 | 0.1902 | 0.1765 | 0.1624 | 0.1579 | 0.1965 | |
| ΔE_{QA} | (mm/s) | 0.0039 | 0.0079 | 0.0079 | -0.0891 | -0.1149 | 0.0956 | |
| ΔE_{QB} | (mm/s) | 0.008 | -0.0201 | -0.0095 | 0.0015 | 0.0337 | 0.0553 | |
| H_{fA} | (T) | 48.9233 | 45.7147 | 42.4147 | 37.6246 | 34.224 | 28.2309 | |
| H_{fB} | (T) | 52.1258 | 47.3784 | 45.8124 | 43.1075 | 39.4096 | 35.5955 | |
| doublets | | | | | | | | |
| δ_{d1} | (mm/s) | | | | | | 0.2064 | 0.2248 |
| ΔE_{Qd1} | (mm/s) | | | | | | 1.2743 | 0.5467 |
| δ_{d2} | (mm/s) | | | | | | | 0.3114 |
| ΔE_{Qd2} | (mm/s) | | | | | | | 2.2531 |

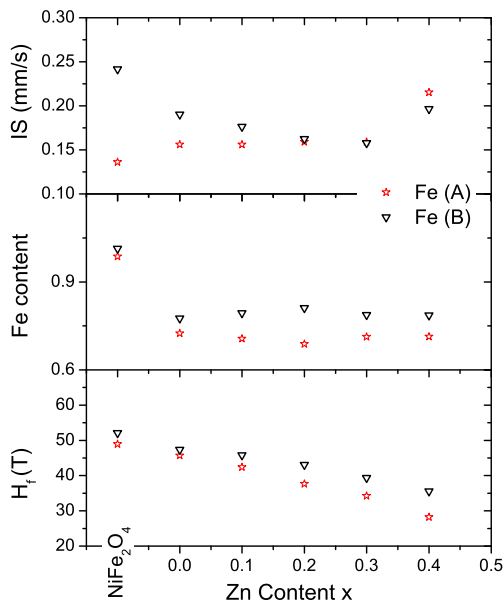


Fig. 4 The isomer shift δ , Fe content, and the hyperfine field (H_f) obtained from the Mössbauer effect measurements for NiFe_2O_4 and $\text{Ni}_{1-x}\text{Zn}_x\text{Ga}_{0.5}\text{Fe}_{1.5}\text{O}_4$ samples

cationic charge, and crystal-field effects [8]. Although Mössbauer effect spectroscopy is only sensitive for the Fe ions in the samples, we used the Fe^{3+} content in the A- and B- sites (Fig. 4) as a building block to the whole cation distribution picture. For Ni ferrite, it is straightforward; only Fe and Ni should be distributed between the A and B sites. It is well established that Ni ferrite is an inverse spinel ferrite, where Ni^{2+} ions occupy the B- site and Fe^{3+} ions distribute equally between the A- and B- sites. Depending on Fe content in both sites, the rest available places will be filled with Ga or Zn ions. The suggested cation distribution is summarized in Table 4. For $x = 0$ sample, we considered Ni ions in the B- site and Ga ions are distributed between both sites. However, introducing Zn makes the situation more complicated. Zn ferrite is known to be normal spinel; Zn^{2+} ions

Table 4 The cation distribution of NiFe_2O_4 and $\text{Ni}_{1-x}\text{Zn}_x\text{Ga}_{0.5}\text{Fe}_{1.5}\text{O}_4$ samples

| Zn content (x) | Cation distribution | |
|---------------------------|---|--|
| | (A)- site | [B]- site |
| NiFe_2O_4 | $\text{Fe}_{0.99}\text{Ni}_{0.01}$ | $\text{Fe}_{1.01}\text{Ni}_{0.99}$ |
| 0. | $\text{Fe}_{0.72}\text{Ga}_{0.28}$ | $\text{Fe}_{0.78}\text{Ni}_{0.22}\text{Ga}_{0.22}$ |
| 0.1 | $\text{Fe}_{0.71}\text{Zn}_{0.1}\text{Ga}_{0.19}$ | $\text{Fe}_{0.79}\text{Ni}_{0.9}\text{Ga}_{0.31}$ |
| 0.2 | $\text{Fe}_{0.69}\text{Zn}_{0.2}\text{Ga}_{0.11}$ | $\text{Fe}_{0.81}\text{Ni}_{0.8}\text{Ga}_{0.39}$ |
| 0.3 | $\text{Fe}_{0.71}\text{Zn}_{0.2}\text{Ga}_{0.09}$ | $\text{Fe}_{0.79}\text{Ni}_{0.7}\text{Zn}_{0.1}\text{Ga}_{0.41}$ |
| 0.4 | $\text{Fe}_{0.71}\text{Zn}_{0.29}$ | $\text{Fe}_{0.79}\text{Ni}_{0.6}\text{Zn}_{0.11}\text{Ga}_{0.5}$ |
| 0.5 ^a | $\text{Fe}_{0.7}\text{Zn}_{0.3}$ | $\text{Fe}_{0.8}\text{Ni}_{0.5}\text{Zn}_{0.2}\text{Ga}_{0.5}$ |

^aAn estimated cation distribution for $x = 0.5$

have strong preference to occupy A-site. For some preparation methods, Zn ion substitutes Fe in the B- site and cause a degree of inversion in Zn ferrite [12–14]. In our case, for small x concentration ($x < 0.3$), Zn is situated as expected in the A- site and transfer Ga from A- to B- site. However, for $x > 0.3$ and since Mössbauer effect measurements suggest an almost equal distribution of Fe between A- and B- sites, therefore Zn ions would substitute Ni in B-site.

3.4 VSM Measurements

Vibrating sample magnetometer (VSM) measurements of NiFe_2O_4 and $\text{Ni}_{1-x}\text{Zn}_x\text{Ga}_{0.5}\text{Fe}_{1.5}\text{O}_4$ samples are shown in Fig. 5. The magnetic parameters obtained from the M-H curves such as saturation magnetization (M_s) and coercivity (H_c) are summarized in Table 5. The saturation magnetization M_s and coercivity H_c are plotted in Fig. 6. M_s is found to increase by the initial replacement of Fe^{3+} by Ga^{3+} and then it decreases slightly for $x \leq 0.2$. However, for $x \geq 0.3$, M_s decreases rapidly. From the measured saturation magnetization, the observed magnetic moment (μ_{obs}) per formula unit in Bohr magneton (μ_B) is given by the following [9]:

$$\mu_{\text{obs}} = MW \times \frac{M_s}{5,585} \tag{7}$$

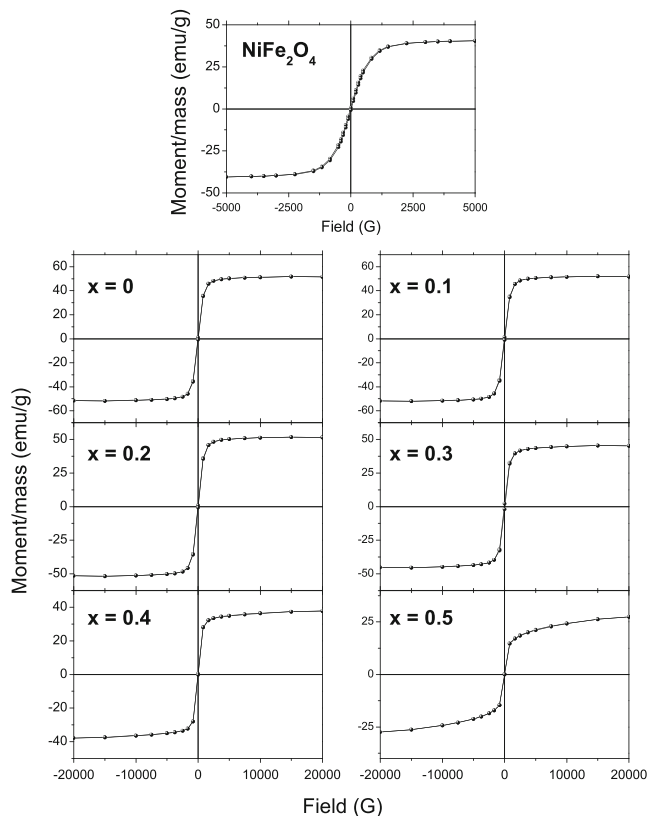


Fig. 5 Magnetic hysteresis loops for NiFe_2O_4 and $\text{Ni}_{1-x}\text{Zn}_x\text{Ga}_{0.5}\text{Fe}_{1.5}\text{O}_4$ samples at room temperature

Table 5 Saturation magnetization (M_S) coercivity (H_c), cation distribution, observed moment μ_{obs} , and calculated moment μ_{cal} of NiFe_2O_4 and $\text{Ni}_{1-x}\text{Zn}_x\text{Ga}_{0.5}\text{Fe}_{1.5}\text{O}_4$ samples

| Zn content (x) | M_S (emu/g) | H_c (G) | $\mu_{\text{obs}}(\mu_B)$ | $\mu_{\text{cal}}(\mu_B)$ |
|---------------------------|---------------|-----------|---------------------------|---------------------------|
| NiFe_2O_4 | 40.49 | 13.798 | 1.69489 | 2.06 |
| 0. | 51.773 | 41.241 | 2.2274 | 2.2565 |
| 0.1 | 52.045 | 27.115 | 2.24469 | 2.2365 |
| 0.2 | 51.751 | 20.064 | 2.23756 | 2.215 |
| 0.3 | 45.368 | 15.215 | 1.96645 | 1.7765 |
| 0.4 | 37.748 | 10.272 | 1.64021 | 1.56476 |
| 0.5 | 27.432 | 5.1375 | 1.19491 | 1.4 |

where MW is the molar weight of the samples. On the other side, the magnetization can be calculated using Néel's model and depending on the cation distribution obtained from ME measurements. According to Néel's model, the μ_{cal} is the vector sum of the magnetic moments of the individual (A) and [B] sublattices:

$$\mu_{\text{cal}} = M_B - M_A \quad (8)$$

The only magnetic ions in $\text{Ni}_{1-x}\text{Zn}_x\text{Ga}_y\text{Fe}_{2-y}\text{O}_4$ system are Ni^{2+} and Fe^{3+} and have magnetic moments $2 \mu_B$ and $5 \mu_B$, respectively. For complete inverse Ni ferrite, the cation distribution is $(\text{Fe}^{3+})[\text{Ni}^{2+}\text{Fe}^{3+}]\text{O}_4^{2-}$ and μ_{cal} will be exact $2 \mu_B$. The μ_{cal} calculated using the cation distribution obtained from ME results is shown in Table 5.

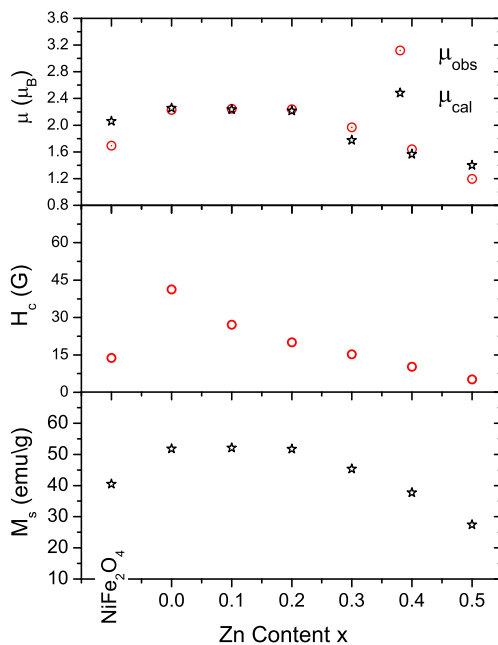


Fig. 6 Variation of saturation magnetization M_S and coercivity H_c for the NiFe_2O_4 and $\text{Ni}_{1-x}\text{Zn}_x\text{Ga}_{0.5}\text{Fe}_{1.5}\text{O}_4$ samples. In the upper panel, a comparison between the observed moment μ_{obs} obtained from the saturation magnetization M_S and the calculated moment μ_{cal} obtained from the Néel model. We used the cation distribution deduced from the Mössbauer effect measurements

Figure 6 represents the comparison between μ_{obs} and μ_{cal} . The values and the behavior of the calculated moments are in good agreement with the observed moments, which strongly support the cation distribution suggested by the Mössbauer effect measurements. As indicated in Fig. 6, the coercivity H_c initially increases by introducing Ga^{3+} ions and then decreases with increasing Zn content x . H_c depends on anisotropy constant, K . By increasing Zn content, which has low anisotropy constant value compared to Ni, H_c is expected to decrease [15].

4 Conclusion

Ni-Ga-Zn ferrite samples are synthesized using solid-state reaction technique and found to have a single-phase cubic spinel. The structural and magnetic properties have been studied with different techniques. These properties were found to be influenced by the Ga and Zn substitution. Mössbauer effect results showed that Ga^{3+} ion substitutes Fe^{3+} in both A and B- sites. For low Zn content, Zn^{2+} goes to A- site but for $x \geq 0.3$, unusually, it distributes between both A- and B- sites. Depending on this cation distribution, the calculated lattice parameter a_{th} and the calculated moment μ_{cal} are in very good agreement with the observed values from XRD and VSM measurements.

References

- Igarash, H., Okazaki, K., Am, J.: Ceram. Soc. **60**, 51 (1977)
- Ata-Allah, S.S., Fayek, M.K., Sayed, H.A., Yehia, M.: Mater. Chem. Phys. **92**, 278 (2005)
- Birajdar, D.S., Mane, D.R., More, S.S., Kawade, V.B., Jadhav, K.M.: J. Mater. Lett. **59**, 2981 (2005)
- Dixit, G., Pal Singh, J., Srivastava, R.C., Agrawal, H.M.: J. Magn. Magn. Mater. **324**, 479 (2012)
- Ata-Allah, S.S.: J. Solid State Chem. **177**, 4443 (2004)
- Kanno, R., Kawamoto, N., Takeda, Y., Masegawa, M., Yamamoto, O., Kinomura, N.: J. Solid State Chem. **96**, 397 (1992)
- Lange's Handbook of chemistry, John A. Dean, McGRAW-HILL, INC (1999)
- Lakhani, V.K., Pathak, T.K., Vasoya, N.H., Modi, K.B.: Solid State Sci. **13**, 539 (2011)
- Yehia, M., Ismail, S.M., Hashhash, A., Supercond, J.: Nov. Magn. **27**, 771 (2014)
- Yehia, M., Labib, Sh., Ismail, S.M.: Physica B **446**, 49 (2014)
- Ata-Allah, S.S., Fayek, M.K., Yehia, M., Magn. J.: Magn. Mater. **279**, 411 (2004)
- Tanaka, K., Makita, M., Shimizugawa, Y., Hirao, K., Soga, N., Phys. J.: Chem Solids **59**(9), 1611 (1998)
- Šepelák, V., Steinike, U., Uecker, D.Chr., Wißmann, S., Beckerà, K.D.: J. Solid State Chem. **135**, 52 (1998)
- Anantharaman, M.R., Jagatheesan, S., Malini, K.A., Sindhu, S., Narayanasamy, A., Chinnasamy, C.N., Jacobs, J.P., Reijne, S., Seshan, K., Smits, R.H.H., Brongersma, H.H.: J. Magn. Magn. Mater **189**, 83 (1998)
- Najmoddin, N., Beitollahi, A., Kavas, H.S., Mohseni, S.M., Rezaie, H., Åkerman, J., Toprak, M.S.: J. Ceram. Inter. **40**, 3619 (2014)